Application of the fundamental measure density functional theory to the adsorption in cylindrical pores

Susana Figueroa-Gerstenmaier
Departament d'Enginyeria Química, ETSEQ, Universitat Rovira i Virgili, Avinguda dels Països Catalans 26, Tarragona 43007, Spain

Felipe J. Blas
Departamento de Física Aplicada, Facultad de Ciencias Experimentales, Universidad de Huelva, Huelva 21071, Spain

Josep Bonet Avalos and Lourdes F. Vega
Departament d'Enginyeria Química, ETSEQ, Universitat Rovira i Virgili, Avinguda dels Països Catalans 26, Tarragona 43007, Spain

(Received 13 March 2002; accepted 26 September 2002)

In this work we have implemented the fundamental-measure density functional theory due to Kierlik and Rosinberg to describe the adsorption of Lennard-Jones molecules in cylindrical pores. The accuracy of the theory in predicting adsorption isotherms and particle density profiles is checked by comparison with grand canonical Monte Carlo simulations for a wide range of pore sizes, showing very good agreement in all cases. In addition, the theory has been applied to the adsorption in slitlike pores to study the influence of the pore geometry on this property. The results indicate that the confinement of the cylindrical geometry introduces significant differences in the shape of the adsorption isotherms and density profiles. These differences are relevant for the characterization of porous materials. © *2003 American Institute of Physics.* [DOI: 10.1063/1.1522393]

I. INTRODUCTION

The thermodynamic and structural properties of inhomogeneous classical fluids constitute a fundamental problem for physics and chemistry. During the last years a great effort has been devoted to the molecular modeling of these properties within the framework of interfacial phenomena, freezing, fluids in confined geometry, etc. Despite the important advances achieved with the combination of modern theories and computer molecular simulations, inhomogeneous situations are not yet completely understood. Even simple spherical fluids show a complex behavior when confined in well-defined geometries. When the pore size is of the order of the correlation length, the presence of walls causes a dramatic change in the behavior of these confined systems compared to that exhibited in the bulk phase. In particular, energetic interactions and geometrical confinement modify the character of phase transitions, shift critical points, and new observable metastable states and hysteresis phenomena appear, among other features.[1]

A very successful and general method for determining the thermodynamic and structural properties of inhomogeneous fluids is undeniably density functional theory (DFT).[2] This method is based on the formulation of the free energy for an inhomogeneous fluid as a functional of the spatially varying one-particle density $\rho(\mathbf{r})$. The density functional approach provides all relevant thermodynamic functions, such as surface tension, solvation forces, adsorption isotherms, density profiles, etc. Unfortunately, the exact free energy functional is only known for a few simple models and, consequently, the cornerstone of the theory is to provide suitable approximations for the free energy.[2]

It is customary to separate the ideal from the excess contributions to the free energy. Moreover, the excess free energy functional is further split, somewhat arbitrarily, into two parts: the hard-sphere contribution and the attractive part usually treated under the mean-field approximation. Within this framework, density functional approaches are further classified into local and nonlocal theories, depending on how the hard-sphere contribution to the excess free energy density is modeled. In the local approximation, the excess free energy density at a point $\mathbf{r}$ is formulated as dependent on the local particle density at the same position $\mathbf{r}$. Although local theories can adequately describe relevant properties in inhomogeneous situations,[3–9] this formulation fails when predicting oscillatory density profiles, such as those observed in confined fluids, since short-range correlations are neglected.[2] On the other hand, in the nonlocal or weighted density functional theories, the excess free energy for the hard-sphere reference system is function of the particle density in the neighborhood of the point $\mathbf{r}$ through smoothed densities. The latter are constructed from appropriate averages of the particle density over a given local volume, thus accounting for the short-range correlations. Different recipes of the weighted density can be found in the literature.[10–21]

A new kind of nonlocal free energy density functionals has been developed in the last two decades. The fundamental-measure theory free energy functional (hereafter referred to as FMT) was originally proposed by Rosenfeld[22] in 1989. This procedure is based on the convolution decomposition of the excluded volume for a pair of convex hard spheres in terms of characteristic functions for the geometry of the two individual bodies. In the original formulation,[22] the excess free energy density of the hard-sphere fluid is obtained from four scalar and two vector

weighting density-independent functions. Later on, Kierlik and Rosinberg[23] proposed a new fundamental-measure functional, defined by only four scalar weighting functions. Although the functional forms of the Rosenfeld and Kierlik and Rosinberg theories are different, it has been proved that both approaches represent the same fundamental density functional.[24]

Most of the initial studies on confined fluids for slitlike and cylindrical pores were based on the local approximation for the repulsive part of the Helmholtz free energy.[25–33] After the work of Nordholm and co-workers[10–13] and Tarazona,[15] in which the nonlocal approach was introduced, a great number of studies based on this approximate method have been undertaken.[34–37] In the past decade, following the work of Rosenfeld and that of Kierlik and Rosinberg, a number of analyses have been directed to study the adsorption behavior of spherical fluids and their mixtures, all of them, however, restricted to slitlike pores.[38–47] As far as dimensional crossover is concerned, more recently Gonzalez *et al.*[48] studied the behavior of a system confined in a spherical cavity with an analysis based on the modifications introduced by Rosenfeld *et al.*[49] on the original work of Rosenfeld.[22] Tarazona,[50] in turn, developed a FMT functional that is able to correctly account for dimensional crossover. To our knowledge, none of the fundamental-measure approach versions has ever been used to describe the behavior of confined fluids in cylindrical geometries. This application, however, has a particular importance since DFT is currently being used to obtain the pore-size distribution from adsorption isotherms in porous materials, in which cylindrical pores are common.[51] Thus, to establish the validity of this kind of functionals for predicting the adsorption behavior in cylindrical pores becomes a matter of fundamental interest.

The main goal of this work is to analyze the ability of the FMT free energy functional, proposed by Kierlik and Rosinberg, to describe the thermodynamic and structural properties of a Lennard-Jones (LJ) spherical fluid confined in cylindrical pores. In particular, the accuracy of the FMT results is tested by comparing them to those obtained from grand canonical Monte Carlo (GCMC) simulations using the same molecular model and for a wide range of pore sizes, from micropores to mesopores. In addition, the effect of the geometrical confinement on the adsorption properties is studied comparing the FMT results for cylindrical pores with the data obtained for slitlike pores of similar width.

The rest of the paper is organized as follows: In Sec. II we briefly review the FMT, we set out the model potentials and approximations used in this work, we define the pore properties, and finally, we give details about the molecular simulations performed. In Sec. III we present and discuss our results. Finally, Sec. IV is dedicated to summarize the main conclusions that can be drawn from this work.

II. METHODOLOGY

A. Density functional theory

In the formulation of the DFT used along this paper we essentially follow the work by Kierlik and Rosinberg.[23] With the aim at studying the adsorption of LJ particles on cylindrical pores, it is convenient to work under constant chemical potential μ. Therefore, we will focus our attention on the grand potential of the system, defined from the Helmholtz free energy according to

$$\Omega[\rho(\mathbf{r})] \equiv F[\rho(\mathbf{r})] - \int dr \rho(\mathbf{r})[\mu - \phi_{\text{ext}}(\mathbf{r})], \tag{1}$$

where the first term on the right-hand side is the intrinsic Helmholtz free energy functional, and in the second term the expression $\phi_{\text{ext}}(\mathbf{r})$ takes into account the potential imposed by the wall.

In the FMT formulation the grand potential hence takes the form

$$\begin{aligned}\Omega[\rho(\mathbf{r})] = {} & k_B T \int d\mathbf{r}\, \rho(\mathbf{r})[\ln(\Lambda^3 \rho(\mathbf{r})) - 1] \\ & + k_B T \int d\mathbf{r}\, \Phi(\{\overline{n}_\alpha(\mathbf{r})\}) \\ & + \tfrac{1}{2} \int d\mathbf{r} \int d\mathbf{r}'\, \rho(\mathbf{r}) \rho(\mathbf{r}') \phi_{\text{att}}(|\mathbf{r} - \mathbf{r}'|) \\ & - \int d\mathbf{r}\, \rho(\mathbf{r})[\mu - \phi_{\text{ext}}(\mathbf{r})].\end{aligned} \tag{2}$$

In this expression, the first term stands for the ideal gas contribution to the free energy. The second term is the excess free energy of the hard-sphere reference system in a weighted density approximation.[23] The third term describes the effect of the attractive interactions between particles, ϕ_{att}, introduced in a mean-field way. The functional dependence of ϕ_{att} stresses the fact that we will only consider here isotropic interactions. The last term represents the contribution of the bulk chemical potential as well as the effect due to the walls of the pore, introduced through the external field $\phi_{\text{ext}}(\mathbf{r})$. Λ is the de Broglie wavelength, k_B is Boltzmann's constant and T is the absolute temperature.

According to Kierlik and Rosinberg,[23] the excess free-energy density of the reference system of hard spheres, $k_B T \Phi(\{\overline{n}_\alpha(\mathbf{r})\})$, is assumed to be a function of the weighted densities, the latter defined as

$$\overline{n}_\alpha(\mathbf{r}) = \int d\mathbf{r}'\, \omega^{(\alpha)}(\mathbf{r} - \mathbf{r}') \rho(\mathbf{r}'), \tag{3}$$

with $\alpha = 0$, 1, 2, and 3. The four weight functions $\omega^{(\alpha)}(\mathbf{r})$ are related to the Heaviside step function, $\Theta(\mathbf{r})$, and its derivatives. These weight functions are independent of the density, and their expression can be found in Ref. 23. In particular, the hard-sphere excess free energy has the form[23]

$$\Phi(\{\overline{n}_\alpha\}) = -\overline{n}_0 \ln(1 - \overline{n}_3) + \frac{\overline{n}_1 \overline{n}_2}{1 - \overline{n}_3} + \frac{1}{24\pi} \frac{\overline{n}_2^3}{(1 - \overline{n}_3)^2}. \tag{4}$$

In choosing this particular recipe of DFT, we take into account several facts; the excess free energy contribution of the reference system of hard spheres is further expressed in terms of fundamental geometrical measures of the particles,[22,23] and its predictions of the structural and thermodynamic properties of the fluid are obtained as consequences

of the theory itself, without further assumptions common to other theories.[2] This DFT for the hard-sphere fluid might be considered as a generalization of the SPT[52,53] free energy to nonuniform situations. Another advantage of this DFT recipe is that the density-independent expression of the weighting functions avoids the need to calculate them anew for each point in the pore. Moreover, the extension to mixtures is straightforward, and specific versions are designed to deal with the crossover to one and zero-dimensional systems.[49,50]

At this point, the equilibrium properties of the fluid can be obtained by minimizing the grand potential functional, Eq. (2), with respect to the local density, at constant chemical potential, μ, and under appropriate boundary conditions.[54] The above requirements result in the Euler–Lagrange equation

$$\mu = k_B T \ln(\Lambda^3 \rho(\mathbf{r}'')) + \int d\mathbf{r} \sum_{\alpha} \omega^{(\alpha)}(|\mathbf{r}-\mathbf{r}''|) \frac{\partial \Phi}{\partial \overline{n}_{\alpha}(\mathbf{r})} + \int d\mathbf{r}\, \rho(\mathbf{r})\, \phi_{\mathrm{att}}(|\mathbf{r}-\mathbf{r}''|) + \phi_{\mathrm{ext}}(\mathbf{r}''), \tag{5}$$

which is an implicit relationship to be satisfied at every space point $\mathbf{r}''$, whose functional inversion yields the density profile in terms of the chemical potential, the attractive and external potential fields and the geometry of the particles.

The inversion of Eq. (5) in the case of a fluid adsorbing onto cylindrical walls of diameter H, unbounded in the axial direction, constitutes the main computational effort of this work. Some details on the numerical procedure employed to solve the convolutions expressed in Eq. (5) are given in the appendix. It is important to realize that our procedure respects the geometrical properties of the system, which is especially relevant near the axis of the cylinder, where the radius of curvature of the ''slices'' of constant density is of the same order of magnitude as the radius of the particles themselves.

B. Molecular model

We have performed FMT density functional calculations as well as GCMC simulations of adsorption in cylindrical pores of different diameter sizes. We have also calculated adsorption properties in slitlike pores using FMT. The molecular parameters used were the same as in the simulation of nitrogen adsorption on model porous glasses of silica.[55,56] Adsorption was assumed to take place on standard conditions for the nitrogen at the normal boiling temperature of 77.4 K. The reason of such a choice is the interest of further applications of our methodology to the determination of the pore-size distribution in these kinds of materials. In some specific cases, we have calculated the adsorption, desorption, and stable branches, as discussed later. For the rest of the cases we have calculated only the adsorption branch.

1. Fluid-fluid interactions

In this work, the nitrogen molecule is modeled as a spherical LJ particle, with a ''cut-and-shifted potential,'' $\phi^{\mathrm{LJ}}(r)$. The LJ parameters ε and σ have been taken from literature[57] (see also Table I). In addition, all the LJ interactions were truncated at a cutoff radius $r_c = 2.52\sigma$.

TABLE I. Parameters of the intermolecular potentials.

Parameter	Fluid–fluid (Ref. 60)	Solid–solid (Ref. 64)	Solid–fluid
σ(Å)	3.75	2.7	3.22
ε/k_B(K)	95.2	230	147.9

We divide the potential into repulsive (reference) and attractive (perturbative) components, following the conventional Weeks, Chandler, and Andersen (WCA) perturbation scheme,[58] splitting the potential at the minimum, with $r_{\min} = 2^{1/6}\sigma$. In this approach, the reference system is replaced by a system of hard spheres with a temperature-dependent diameter $d(T^*)$. We have used the mapping from LJ to hard spheres developed by Verlet and Weis[59] and Lu *et al.*,[60] with the coefficients $\eta_1 = 0.3837$, $\eta_2 = 1.035$, $\eta_3 = 0.4249$, $\eta_4 = 1$, fitted by Peterson *et al.*[31] to match the bulk phase diagram of the LJ fluid.

The excess Helmholtz free energy per particle of the reference system, Φ, is taken from the SPT,[52,53] or PY equation of state for the uniform hard-sphere fluid[61–63] [Eq. (4)], where $\rho(\mathbf{r}) \equiv \rho$. Moreover, the weighted densities defined in Eq. (3), which coincide with the variables of the SPT,[52,53] can be written in terms of fundamental measures characterizing the particle ($\overline{n_0} = \rho$, $\overline{n_1} = R\rho$, $\overline{n_2} = 4\pi R^2 \rho$, $\overline{n_3} = \frac{4}{3}\pi R^3 \rho$).

2. Solid–fluid interactions

The LJ parameters for the substrate atoms are those used by Gelb and Gubbins[55,56] following the work from Brodka and Zerda,[64] and they can be found in Table I. These parameters represent bridging oxygen atoms in silica, since previous simulations of adsorption on silica gels show that the omission of the silicon atoms is an acceptable approximation.[64,65] The LJ solid–fluid parameters (Table I) follow the Lorentz–Berthelot mixing rules.

We have represented each pore as an infinite cylinder where the atoms are single spherical LJ sites. These LJ spheres are laid out in six concentric layers separated by a distance Δ. Each layer is arranged in such a way that consecutive rows of solid atoms are displaced 0.15 nm in the angular and axial directions. The distance between the axes that define the successive rows is called d. The resulting overall configuration of each layer can be described as a hexagonal lattice. The values of these parameters are fixed ($d = 0.277$ nm and $\Delta = 0.30$ nm), so that the total density of oxygen atoms in our model, 44.1 atoms/nm^2, and a material porosity of 30%, are approximately mimicked.[56] The pore diameter H is defined from the center of the particles on opposite sides of the innermost layer. An example of this cylinder and the disposition of the atoms can be seen in Fig. 1(a). In the case of slitlike pores, the material is modeled applying the same principles to a planar geometry, where the parameter H represents the distance between two identical parallel walls. In Fig. 1(b) a representation of this pore can be found.

The total potential energy between a fluid molecule probe and the wall is calculated as the sum of the contribu-

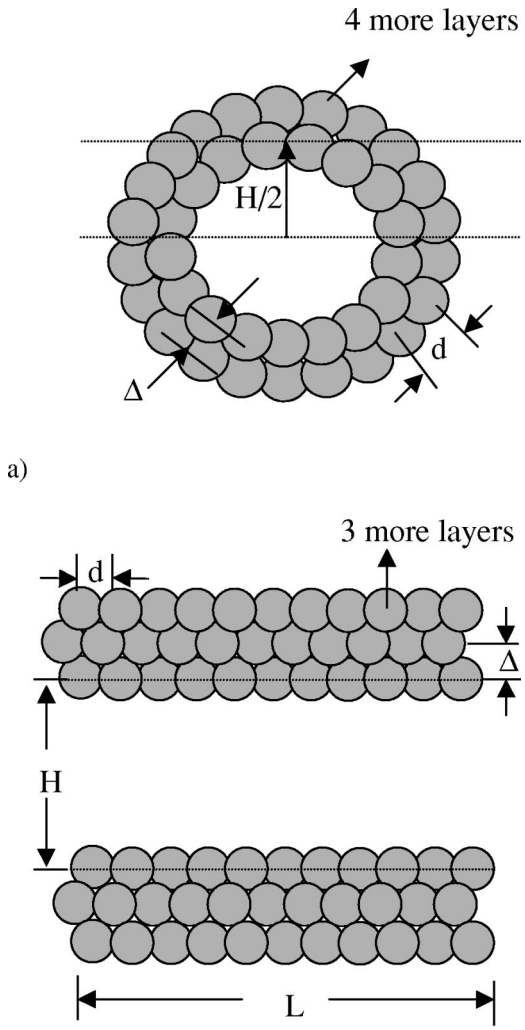

FIG. 1. Structure of the (a) cylindrical and (b) slitlike pores.

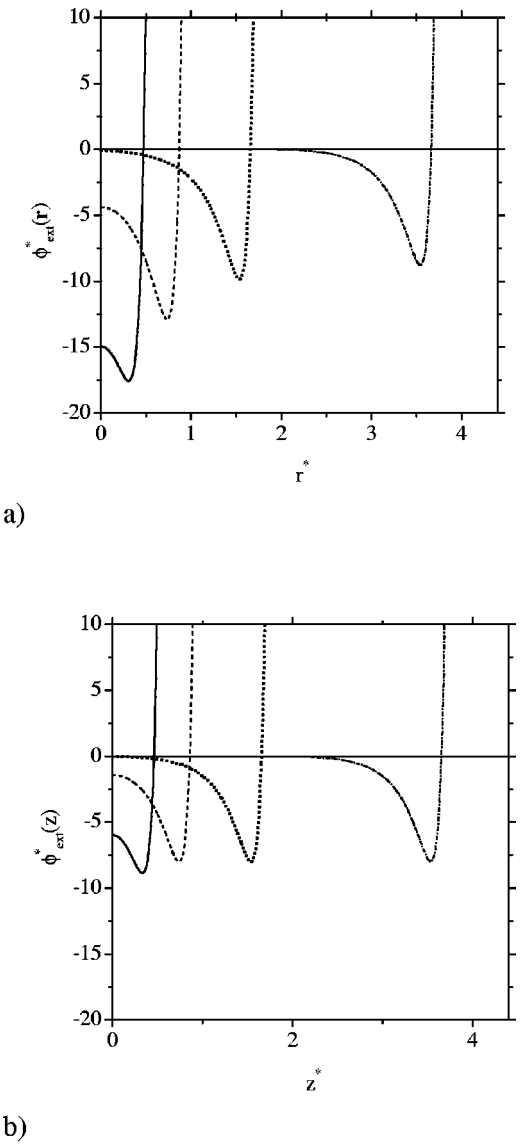

FIG. 2. Dependence of the wall potential as a function of the distance for (a) cylindrical and (b) slitlike pores of different size: $H=2.4\,\sigma$, $3.2\,\sigma$, $4.8\,\sigma$, and $8.8\,\sigma$, starting from left to right.

tions of all the substrate atoms. However, we have considered an averaged potential, constructed from the previous one by integrating with respect to the angular and axial directions, preserving only the radial functional dependence. For slitlike pores, the potential is averaged over translations parallel to the walls.

In Fig. 2(a) we have shown the radial dependence of the cylindrical wall potential, $\phi_{\text{ext}}(r)$, for several pore size diameters. As it can be seen in the figure, the influence of the wall on the adsorption is expected to be very important for pores whose width is comparable with the range of the attractive potential of the wall. In particular, for such narrow pores the adsorbed fluid will have properties significantly different from those of the bulk fluid. Conversely, for wider pores one expects the effect of the pore walls to be important only at low coverage, and capillary condensation to occur at a given critical pressure. In Fig. 2(b) we present the wall potential as a function of the distance in the direction perpendicular to the parallel walls, $\phi_{\text{ext}}(z)$ for slitlike pores of different width.

The mean pore fluid density, $\langle\rho\rangle$, is defined from the relation

$$\langle\rho\rangle=\frac{\int d\mathbf{r}\,\rho(\mathbf{r})}{\int d\mathbf{r}}, \tag{6}$$

where the integral is extended over the volume of the pore and this volume is considered a function of H. The excess density is defined as the deviation of the average density with respect to the bulk values, that is

$$\langle\rho^E\rangle\equiv\langle\rho\rangle-\rho_{\text{bulk}}. \tag{7}$$

C. Monte Carlo simulations

Aiming at a quantitative comparison between the FMT and Monte Carlo simulations, we have chosen to apply the same molecular parameters for both procedures. It is well known that the bulk properties predicted by each methodology are different. However, since both theories are molecular

in nature, we have decided to compare the bare results from the same molecular model and analyze the differences later on. Other authors have compared DFT results with Monte Carlo simulations based on the same bulk properties,[37,66] although such a procedure implies the use of different molecular parameters for each approach. Despite the fact that the latter point of view is legitimate, the different sets of molecular parameters used in that case represent in fact different systems, although very close in their properties.

In our simulations, adsorption isotherms and density profiles have been obtained through a GCMC scheme.[67,68] The temperature T, the volume V, and the chemical potential μ inside the pore are thus fixed. To obtain the adsorption isotherms, we ran the simulations at values of the activity, defined as

$$z=\frac{\exp(\mu/k_BT)}{\sigma}, \tag{8}$$

corresponding to bulk chemical potential, equal to those used in the density functional theory calculations.

Three different types of Monte Carlo trials were used in the simulations: creation of a new adsorbate molecule at a random position inside the pore, removal of a randomly chosen adsorbate molecule, and move of a randomly chosen adsorbate particle. The maximum move for a particle translation was fixed at 0.20σ, and the ratio between trials was fixed to be a 50% for translation moves and the remaining 50% for creation–destruction moves. The length of the simulation box was changed from 6 to 100 nm, depending on the pore diameter size, to ensure a sufficient number of particles inside. In the axial and angular directions, periodic boundary conditions and minimal image convention were applied. The LJ potential was cut and shifted with $r_c=2.52\sigma$. To equilibrate the system, the simulations were run for at least 3×10^6 moves. Averages were then collected from runs over at least 20×10^6 configurations after equilibration. The block size to compute averages was fixed at 500 000 moves.

The excess pore fluid density in this case is defined as

$$\langle\rho^E\rangle=\frac{\langle N\rangle}{V}-\rho_{\text{bulk}}, \tag{9}$$

where $\langle N\rangle$ is the mean number of particles inside pore and V is the pore volume, defined in the same way as in Eq. (6).

III. RESULTS AND DISCUSSION

We have calculated density profiles and adsorption isotherms for cylindrical pores of different sizes by means of two approaches, FMT and GCMC. In addition, FMT calculations for slitlike pores of the same width will serve us to discuss as well the main differences introduced by the dissimilarity in the geometry. The pore diameters studied here are in the range from $H=3.2\sigma$ to 17.6σ, which covers the region from micropores (whose diameter is less than 20 Å), to larger pores (mesopores, with a diameter between 20 and 500 Å). We have found that our numerical implementation of the FMT model used here fails to converge for very narrow pores ($H<3.2\sigma$, corresponding to $H<12$ Å) which constitutes the limit of the applicability of our procedure. An analysis of the strictly 1D[49,50] adsorption is out of the scope of this work. The main points to be discussed in this section will be, on one hand, the comparison of the excess density and density profiles between FMT and GCMC, to elucidate the limits of the agreement of both procedures in the analysis of the adsorption in cylindrical pores, when the same molecular model is used. On the other hand, the effect of the geometry in the profiles and adsorption isotherms will be briefly discussed by comparing the FMT results for cylindrical and slitlike pores. This latter point is of relevance in the calculation of pore-size distributions of real materials from experimental data of adsorption isotherms.

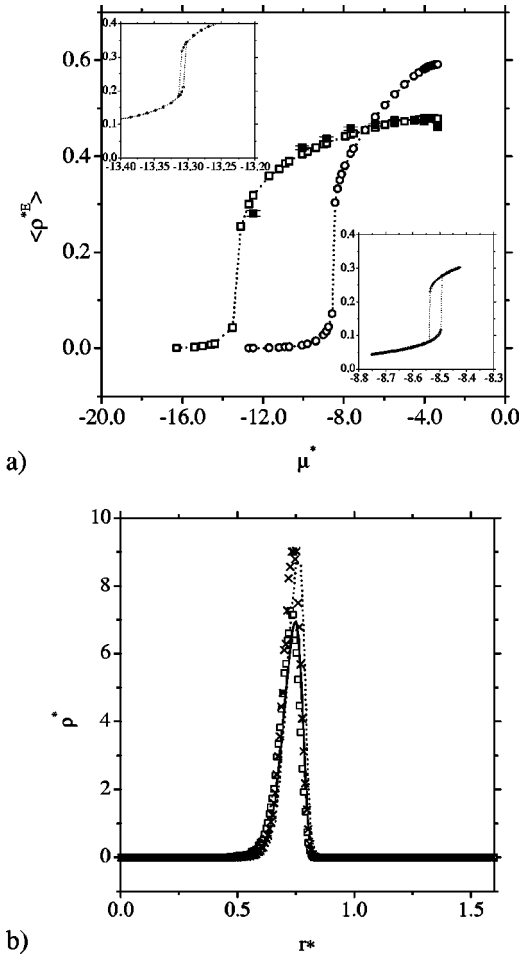

FIG. 3. (a) Adsorption isotherms in $H=3.2\,\sigma$ cylindrical and slitlike pores; open squares, FMT calculations, closed squares, GCMC simulations, both in the cylindrical pore; open circles, FMT calculations in the slitlike pore. The lines are a visual aid. The insets show the hysteresis FMT results in the slitlike pore on the right-hand side and in the cylindrical pore on the left-hand side. (b) Density profiles from FMT calculations (lines) and GCMC simulations (symbols) in the cylindrical pore at $\mu^*=-10.065$ (solid line and open squares), and -4.031 [dotted line and crosses ($\times$)].

Figure 3(a) shows the adsorption isotherm obtained from FMT corresponding to cylindrical and slitlike pores of size $H=3.2\sigma$, as well as the simulation results for the cylindrical geometry. As it can be seen, the agreement between predictions from the theory and simulation data is excellent in the whole range of chemical potentials considered (from $\mu^*=-12.479$ to -3.338), although theoretical predictions slightly underestimate the amount of fluid adsorbed along the

whole adsorption isotherm. Results corresponding to the adsorption in the slitlike pore are significantly different from those obtained for the cylindrical geometry. In the former, a very pronounced jump in the average density is observed at chemical potentials around $\mu^*=-8.0$, followed by a continuous increase of the density as the chemical potential is raised. For the cylindrical pore, the jump in the density is displaced towards lower chemical potentials. At higher chemical potentials, the continuous increase in the density is smoother than in the case of planar geometry. The insets in Fig. 3(a) show the hysteresis existing around the sudden density jump, indicating that it corresponds in both cases to a *first order phase transition* inside the pore. A higher degree of confinement in cylindrical pores is responsible for the appearance of the mentioned transition at chemical potentials significantly lower than in slitlike pores. As seen in Fig. 3(b), only one rather localized annular layer is formed at the wall inside the pore, in the whole chemical potential range studied. Thus, once this layer is build, the increase of the chemical potential only introduces changes in the height of the density profile, yielding to the observed continuous increase of the excess adsorption after the transition in both geometries. The nature of such a transition is not completely clear, since the confinement of the fluid, the curvature of the wall, as well as the fluid–solid potential interactions influence the kind of the transition as well as its location in the space of thermodynamic parameters. However, we attribute this phase transition to the so-called 0 to 1 layering transition, previously found by different authors.[36,69,70] We will come back to this point later on.

The agreement between theoretical FMT predictions and GCMC simulation results in Figs. 3(a) and 3(b) is very good for all thermodynamic conditions, with special emphasis on the localization and the height of the density peaks at different chemical potentials. It must be noted, however, that the agreement between both sets of results is better at low chemical potentials (i.e., pressures). This effect is a consequence of the lack of accuracy of the FMT approach used in this work to predict the adsorption behavior for very narrow pores (which would confine the fluid to an almost one-dimensional behavior). In Fig. 3(a) the differences between the adsorption isotherms of cylindrical and planar pores can be ascribed to the geometrical constraints that crucially determine the way in which molecules accommodate inside confined geometries.

Regarding the adsorption isotherms and density profiles in wider pores, Fig. 4(a) shows the excess adsorbed density versus the chemical potential (adsorption isotherm) of cylindrical and slitlike pores of size $H=4.8\sigma$. The adsorption isotherm corresponding to the cylindrical pore has also been obtained from Monte Carlo simulation. As it can be seen, the theory is able to provide a realistic description of the excess density versus the chemical potential since an almost quantitative agreement between FMT and GCMC results is found in all the range of chemical potentials studied.

More in detail, at low chemical potentials ($\mu^*<-7.0$) a monolayer is formed in both pores. As the chemical potential is increased a second layer is adsorbed in both cylindrical and slitlike pores without the appearance of additional layers.

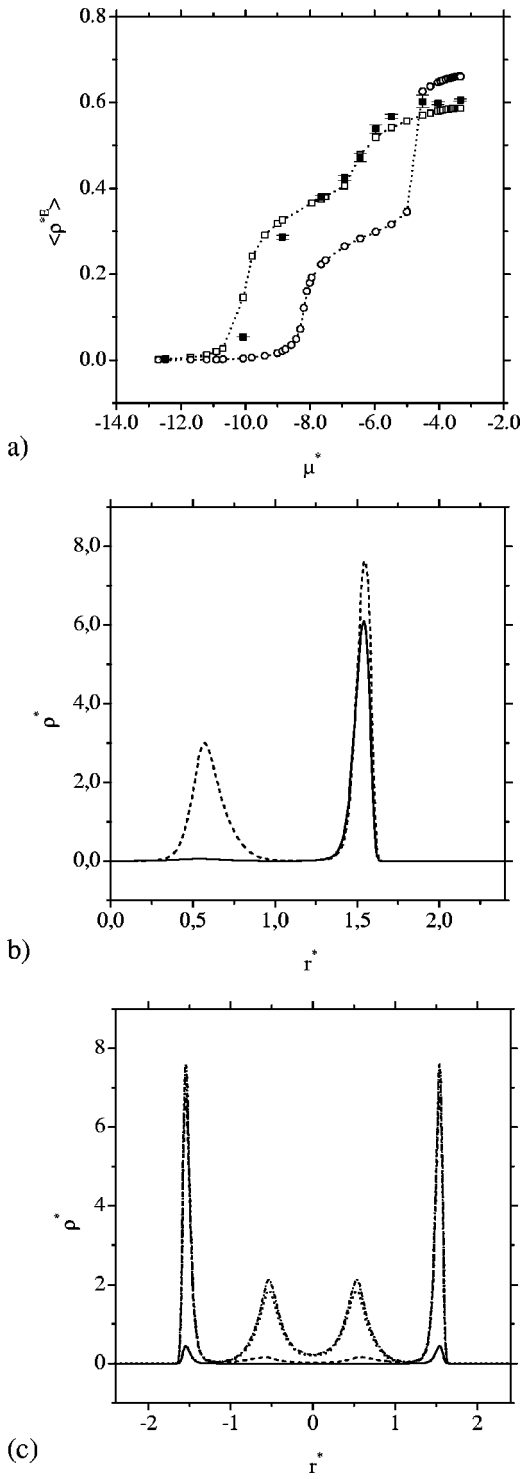

FIG. 4. (a) Adsorption isotherms in $H=4.8\,\sigma$ cylindrical and slitlike pores; the notation is the same as in Fig. 3(a). (b) Density profiles from FMT calculations in the cylindrical pore at $\mu^*=-7.651$ (solid line), and -4.031 (dashed line). (c) Density profiles from FMT calculations in the slitlike pore at six different μ^*, from bottom to top: -10.065, -8.858, -7.651, -4.995, -4.513, -3.338.

However, important differences between the adsorption isotherms can be observed. The excess density in the cylindrical pore is higher than that corresponding to the planar geometry in practically the whole range of chemical potential values (except at the highest chemical potentials). Also, the increase in density observed when a new layer is formed is more

pronounced in the case of the slitlike geometry. This is especially true in the formation of the second adsorbed layer inside the slitlike pore. To elucidate the reasons for this behavior we have also examined the density profiles corresponding to both geometries. Figure 4(b) shows the density profiles, at two different chemical potentials, inside the cylindrical pore. At the lowest chemical potential only a single annular layer is adsorbed, with the density peak located at $r^*=1.5$. This position is consistent with the location of the solid–fluid potential minimum for a cylindrical pore of $H=4.8\sigma$ (see Fig. 2). As the chemical potential is increased, a second adsorbed layer appears close to the center of the cylinder, in agreement with the slight increase of the adsorption isotherm observed in Fig. 4(a).

The isotherm for the planar geometry case, although apparently similar, is in fact qualitatively different from that of the cylindrical pore. Notice, for instance, that in the slitlike pore there are particles in the center of the pore at high chemical potential values [see Fig. 4(c)], whereas molecules are strongly excluded from the axial region of the cylinder. This effect indicates that capillary condensation is likely to occur in the planar geometry but not in the cylinder of the same dimensions $H=4.8\sigma$, in the range of chemical potentials studied here. A detailed analysis of the hysteresis cycle as well as of the free energy indicates that the jump in the excess density in the planar geometry corresponds to a first order phase transition that can be described as capillary condensation.[5] In the case of cylindrical geometry, the formation of the second layer does not correspond to thermodynamic phase transition but merely to a continuous filling of the second layer. In fact, it is worth noting that the average density is proportional to the first derivative of the free energy [Eq. (2)] with respect to the chemical potential, but the average density does not present a discontinuity, nor does its slope diverge.

In the planar pore one can also notice the formation of the first layer around $\mu^*=-8$, a slightly higher chemical potential than in the $H=3.2\sigma$ pore. This effect is dominated by the solid–fluid interaction as it can be seen by the fact that it appears at the same chemical potential for all slitlike pores of larger width. However, this transition cannot be considered as being of first order. In fact, in this case, no hysteresis in the average density is observed around this value of chemical potential, being this quantity (related to the first derivative of the free energy) continuous across the transition, up to the accuracy of our numerical method. The sharp slope observed, however, could indicate that the behavior could correspond to a continuous second order phase transition. In the case of the cylindrical geometry, the transition is observed at lower chemical potential and seems to also display such a continuous character.

In the mesopore range we present results for two pore sizes, $H=8.8\sigma$ and 17.6σ, which correspond, respectively, to the series of Figs. 5(a)–5(c) and 6(a)–6(d). In Fig. 5(a) we show the adsorption isotherms for cylindrical and slitlike pores of width $H=8.8\sigma$. The agreement between the theoretical adsorption isotherm and simulation data corresponding to this cylindrical pore is better than that obtained for narrower pores, as expected. The adsorption isotherms for both geometries exhibit the same qualitative behavior. One observes, on one hand, the crossover from an empty pore to the formation a monolayer at low chemical potentials, as in the previous cases. This increase in the adsorbance in planar geometries is located at the same chemical potential of about $\mu^*=-8.2$ in all the studied pores with $H>3.2\sigma$. However,

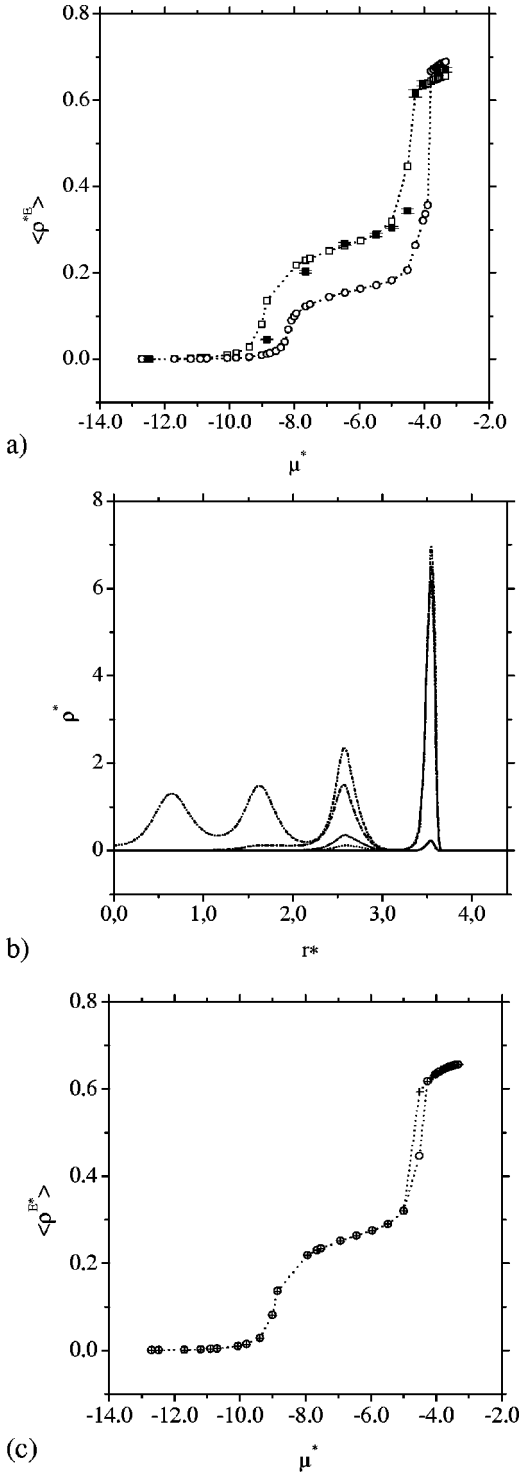

FIG. 5. (a) Adsorption isotherms in $H=8.8\,\sigma$ cylindrical and slitlike pores; the notation is the same as in Fig. 3(a). (b) Density profiles from FMT calculations in the cylindrical pore at five different μ^*, from bottom to top: -10.065, -5.478, -4.995, -4.513, -3.338. (c) Adsorption isotherms in the cylindrical pore by FMT, adsorption and desorption branches.

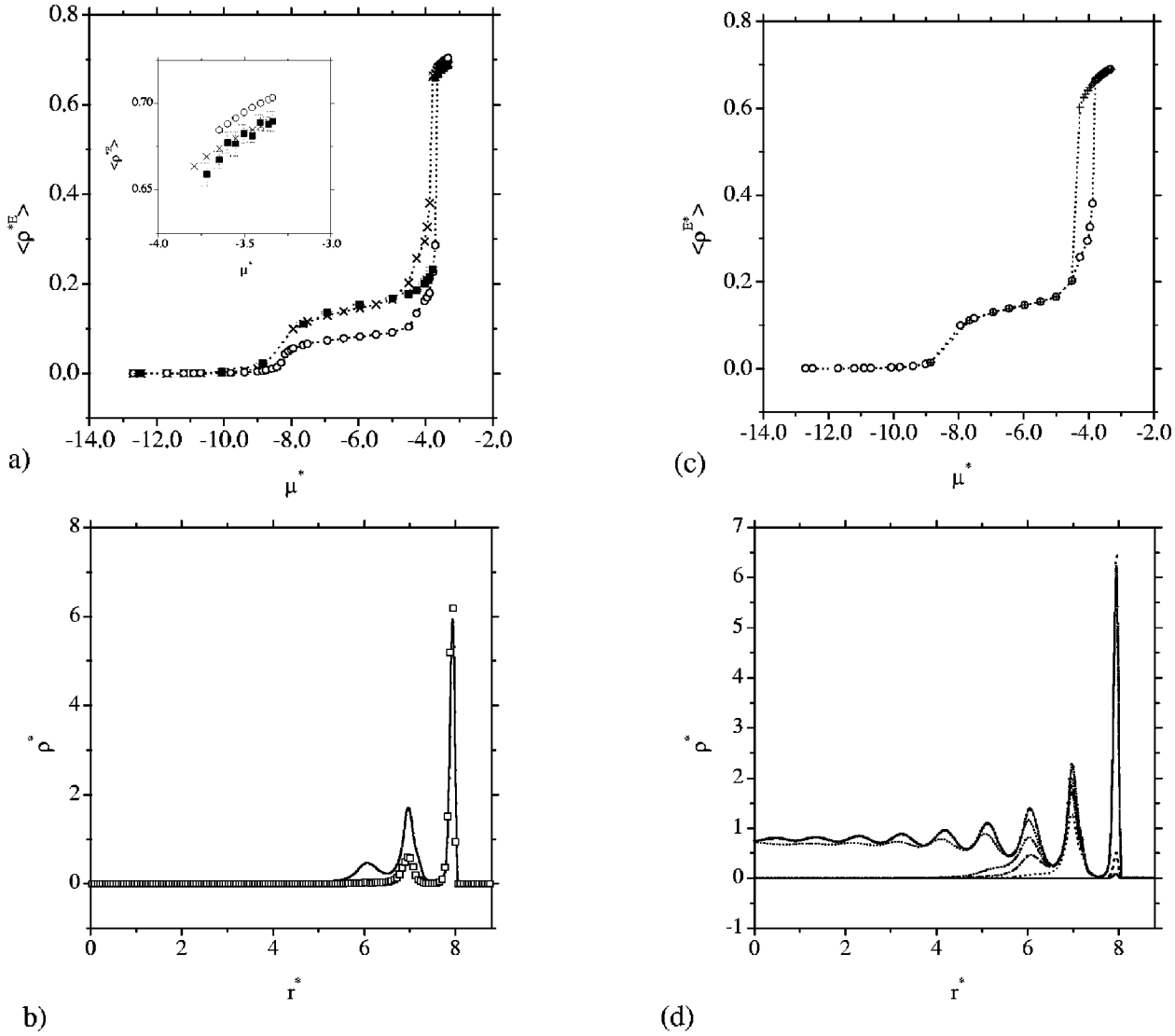

FIG. 6. (a) Adsorption isotherms in $H=17.6\,\sigma$ cylindrical and slitlike pores; the notation is the same as in Fig. 3(a), except that FMT adsorption in cylindrical pores shown as crosses for clarity. Inset shows the details in the high chemical potential region. (b) Density profiles of the cylindrical pore from FMT calculations (lines) and GCMC simulations (symbols) at $\mu^*=-3.959$. (c) Adsorption isotherms in the cylindrical pore by FMT, adsorption and desorption branches. (d) Density profiles from FMT in the cylindrical pore at seven different μ^*, from bottom to top -10.065, -8.858, -4.272, -3.959, -3.887, -3.791, -2.898.

the local curvature of the walls in cylindrical geometry shifts the transition region towards lower chemical potentials as the diameter decreases. In both cases, however, the formation of the thin layer at the wall seems to be continuous and, as before, such a behavior cannot be attributed to a first order phase transition.

On the other hand, the sudden increase in the excess density as the chemical potential is increased corresponds to capillary condensation in both, cylindrical as well as planar geometries. It is important to note that capillary condensation is shifted towards the region of lower chemical potential as the degree of confinement increases, due to both, the change in the geometry (from planar to cylindrical) and by the change in the pore size.[5,25,27]

Notice that, while in cylindrical geometry the agreement between calculated and simulated GCMC results at low chemical potential is excellent above capillary condensation, the values of the predicted excess density from Monte Carlo simulations are higher than those corresponding to the theory for both pore sizes [see Figs. 5(a) and 6(a)]. The choice of the same molecular model leads in fact to a slightly different thermodynamic behavior in the bulk fluid properties. Hence, these differences are expected in a region of the isotherm dominated by the bulk fluid. For these two sizes and below the capillary condensation chemical potential, the excess density predicted for slitlike pores is lower than that corresponding to cylinders. The difference is less noticeable as the pore diameter increases, due to the loss of confinement. As in the previous cases, we have also considered the density profile behavior along the adsorption isotherms. Figure 5(b) shows density profiles corresponding to a cylindrical pore of diameter $H=8.8\sigma$ at different chemical potentials. When capillary condensation occurs, an increase of the density in the central part of the pore takes place. However, due to the higher degree of confinement, the fluid still displays a higher order than in planar geometries under the same conditions.

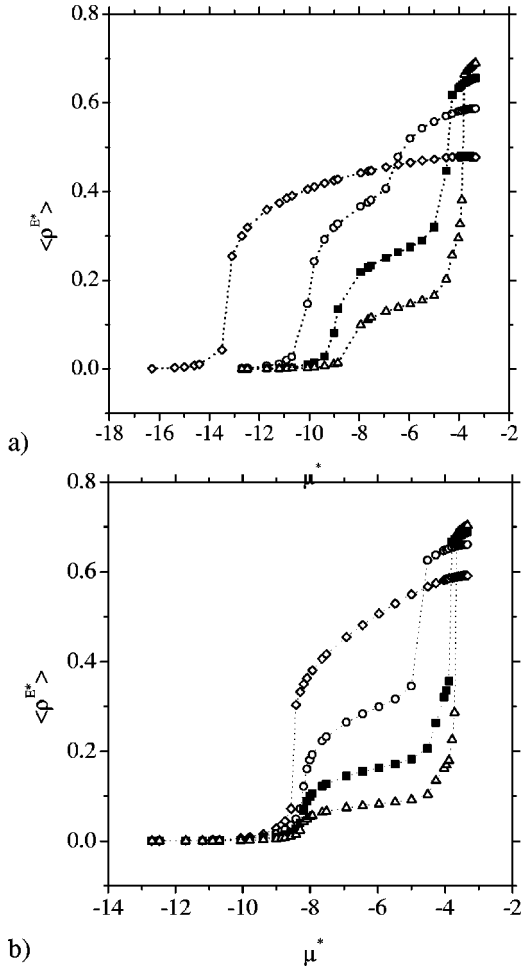

FIG. 7. (a) Adsorption isotherms in cylindrical pores with different diameter: $H=3.2\,\sigma$ (open diamonds), $4.8\,\sigma$ (open circles), $8.8\,\sigma$ (closed squares), and $17.6\,\sigma$ (open triangles); from FMT calculations. (b) The same notation as in (a) but in slitlike pores.

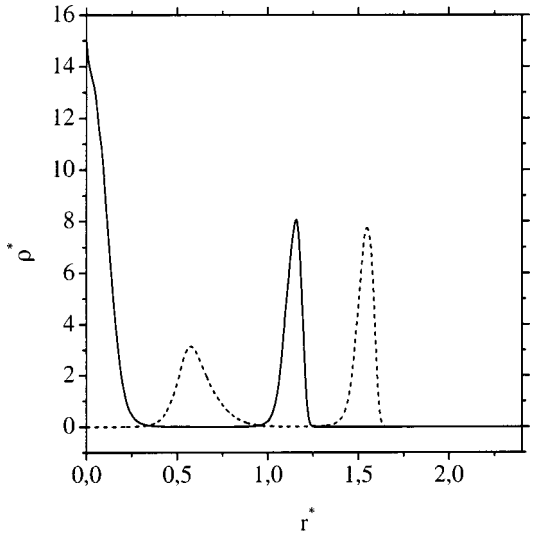

FIG. 8. Density profiles from FMT calculations in $H=4.0\,\sigma$ (solid line), and in $H=4.8\,\sigma$ (dashed line) cylindrical pores at the same chemical potential, $\mu^*=-3.338$.

As it can be seen in Fig. 5(c), the adsorption isotherm in the cylinder exhibits hysteresis, clearly indicating that the discontinuous jump observed in Fig. 5(a) must be ascribed to a gas–liquid phase transition inside the pore.

The adsorption behavior of a second wider mesopore of diameter $H=17.6\sigma$ is analyzed in Figs. 6(a)–6(d). We have also included the adsorption isotherm corresponding to the slitlike pore of the same size [see Fig. 6(a)]. The same qualitative analysis as that regarding the previous pore size can be performed, although the differences between both geometries tend to reduce as the pore size increases. In Fig. 6(b) we compare the density profiles obtained from FMT and simulation for the pore $H=17.6\sigma$ closely underneath capillary condensation ($\mu^*=-3.959$). For this value of the chemical potential, only three layers are distinguishable. The hysteresis cycle is shown separately in Fig. 6(c) for more details. Finally, Fig. 6(d) shows a set of different theoretical density profiles for a sequence of chemical potential values. As can be seen, capillary condensation can be detected when the density profiles change from a gaslike to a liquidlike behavior, giving rise to a finite value of the local density in the central region of the pore.

Figures 7(a) and 7(b) summarize the adsorption isotherms for the four pore sizes analyzed, corresponding, respectively, to cylindrical and planar geometries. In the cylindrical geometry, the smallest pore size, $H=3.2\sigma$, exhibits a behavior completely determined by wall effects, including the first order 0 to 1 layering transition already mentioned. Due to the narrowness of this pore, only a single complete layer of molecules can be accommodated inside the pore. As the pore size is increased, $H=4.8\sigma$, the formation of the first adsorbed layer is located at higher chemical potential than in the $H=3.2\sigma$ and, moreover, seems to be thermodynamically of second order. An additional layer is continuously adsorbed as the chemical potential increases. This effect can be explained as a liquid–liquid enhanced interaction due to the proximity of opposite parts of the cylindrical wall that induces the exclusion of particles in the axial region of the pore and its possible liquidlike behavior and, thus, capillary condensation. A further increase in the pore size, $H=8.8\,\sigma$ and $17.8\,\sigma$, leads to multilayer adsorption with capillary condensation phase transition at high chemical potential. The formation of the first layer corresponds to a continuous behavior and its location is affected by the curvature of the wall, being displaced towards lower chemical potentials as the curvature increases.

In the analysis of the isotherms of pores with planar a geometry, summarized in Fig. 7(b), we have observed that the pore of width $H=3.2\,\sigma$, also exhibits a 0 to 1 first order layering transition, as in the case of cylindrical geometry. However, the formation of the first layer at larger pore widths is located around the same chemical potential, independently of the pore width, and corresponds to a continuum filling with no discontinuity in the first derivative of free energy, but with a large value of the second derivative that could correspond to a divergence. On the other hand, the capillary condensation is shifted by the confinement towards lower chemical potentials and it approaches the bulk liquid–vapor phase transition chemical potential as the pore width increases.

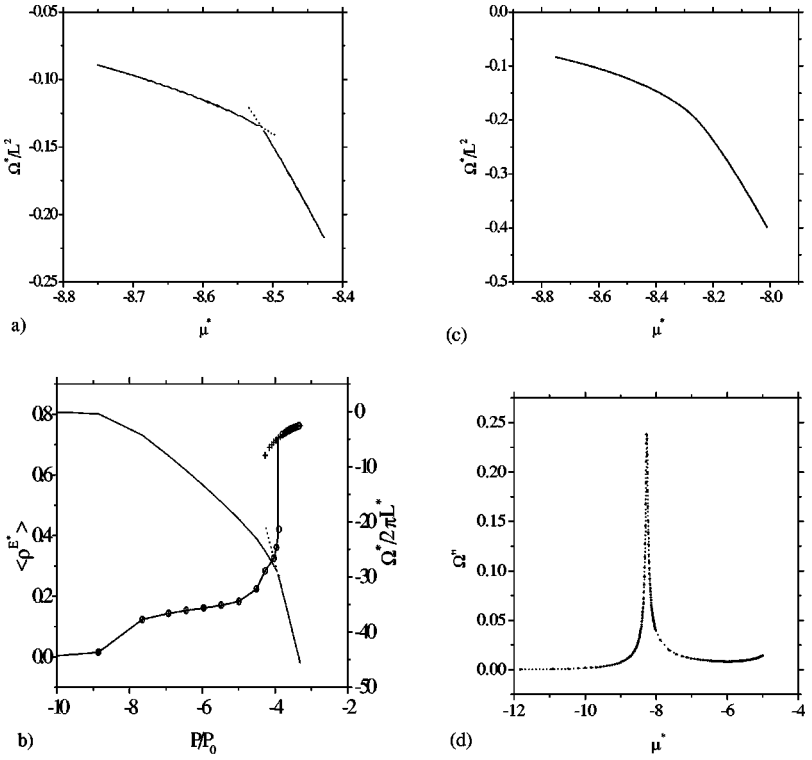

FIG. 9. (a) Changes in the grand-potential energy of the system shown in the inset of Fig. 3(a). FMT calculations in the $H=3.5\,\sigma$ planar pore. (b) Adsorption isotherm (open circles), desorption isotherm (+), and stable isotherm (solid line) in $H=17.6\,\sigma$ cylindrical pore. The zigzag line shows the changes in the grand-potential energy of the system. (c) Changes in the grand-potential energy of the system $H=17.6\,\sigma$ slitlike pore around $\mu^*=-8.0$. (d) Second derivative of the grand-potential energy of the same system in (c).

As an example of the effect of the strong geometrical constraint over the adsorption properties of cylindrical pores, we present the density profiles for different pore widths. In particular, Fig. 8 shows the density profiles corresponding to two cylindrical pores with $H=4.0\,\sigma$ and $4.8\,\sigma$. In the widest pore, geometrical constraints forbid the formation of a layer over the axis of the cylinder, while in the narrowest pore, this layer is strongly favored, showing a peak much higher than the one close to the wall. In slitlike pores, although not represented here, the height of the observed peaks shows a progressive decrease as the molecules approach the center of the pore.

Having described the phenomena observed for various pore sizes, it is worth to separately analyze the behavior of the free energy [Eq. (2)]. We have identified three distinct features in the adsorption isotherms, namely, the first order 0 to 1 layering transition for the narrower pores, capillary condensation, and a sudden increase of the adsorbance due to the formation of dense thin layers at the solid surface. First, as seen in Fig. 3(a), the isotherm for the pore size $H=3.2\,\sigma$ show a weak discontinuity in both cases, indicating the first order nature of the transition.[5] Figure 9(a) shows the behavior of the free energy in the vicinity of this transition for the planar pore, where the discontinuity of the first derivative can be observed, as well as the metastable lines of the free energy. Second, capillary condensation has been described as a shift of the bulk liquid–vapor phase transition, induced by the confinement.[25,27] In Fig. 9(b) we present the free energy of the isotherm corresponding to the cylindrical pore width $H=17.6\,\sigma$ that shows a jump of its first derivative at the location of the capillary condensation transition, which serves to place the physical isotherm between the two metastable branches. Third, the sudden jump in the adsorption isotherm around $\mu^*=-8$, in pores of planar geometry, could be reminiscent of a prewetting phenomenon existing for one wall in an infinite system.[5,71] The detailed analysis of the free energy around this particular chemical potential, for $H=17.6\,\sigma$ [see Fig. 9(c)] seems to indicate that this behavior cannot be attributed to a first order phase transition. The second derivative of the free energy [see Fig. 9(d)] shows a sharp peak that could suggest that the formation of the thin dense layer inside the pore corresponds to a second order phase transition. However, the numerical accuracy of our analysis does not permit us to distinguish whether the peak is a true divergence, corresponding to a second order phase

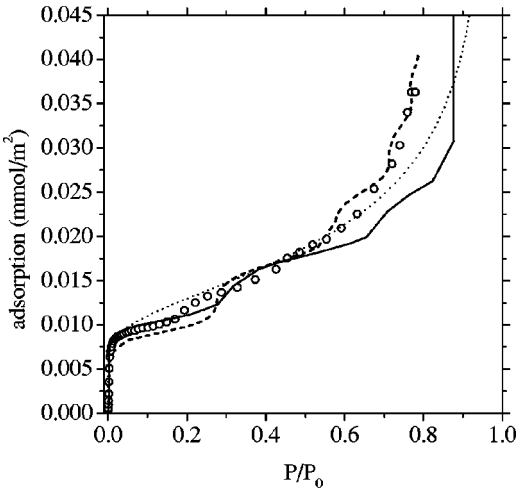

FIG. 10. Adsorption isotherms in $H=90$ Å$(25.18\,\sigma)$ cylindrical pore; solid line, FMT calculations in this work; dashed line, NLDFT calculations (Ref. 47); open circles, GCMC simulations (Ref. 47); dotted line, experimental data on nonporous silica (Ref. 74).

transition, or it is finite, in which case we would identify a mere crossover between two regimes. Even more, the possibility of a very weak first order transition cannot completely be discarded, in view of the thermodynamic behavior associated to the formation of the first layer in the smaller pores analyzed. To be conclusive about the true nature of the transition and the effect of the wall curvature in its location, an exhaustive analysis beyond the scope of this work should be undertaken. Nevertheless, everything seems to indicate that the behavior related to the formation of the thin layer at the wall, in the cases analyzed in this paper, could corresponds to phenomenology expected at the vicinity of a critical point, perhaps related to the critical end point of a prewetting line in an semi-infinite system.

Finally, it is interesting to compare FMT results to those obtained using other formulations of DFT. Figure 10 shows the adsorption isotherm obtained through our DFT formulation, with a cylindrical potential that takes the form[72]

$$\phi_{\mathrm{ext}}(r,\,R)=\pi^2\rho_s\varepsilon_{sf}\sigma_{sf}^2\left[\frac{63}{32}\left[\frac{r}{\sigma_{sf}}\left(2-\frac{r}{R}\right)\right]^{-10}\times F\left[-\frac{9}{2},-\frac{9}{2};1;\left(1-\frac{r}{R}\right)^2\right]-3\left[\frac{r}{\sigma_{sf}}\left(2-\frac{r}{R}\right)\right]^{-4}\times F\left[-\frac{3}{2},-\frac{3}{2};1;\left(1-\frac{r}{R}^2\right)\right]\right], \tag{12}$$

where $F[\alpha,\beta,\gamma;\chi]$ are the hypergeometric functions,[73] and ρ_s is the density of oxygen atoms in the pore wall. Here, R is the radius of the pore of diameter $H=90$ Å $(25.18\,\sigma)$ and σ_{sf} and ε_{sf} are the LJ solid–fluid interaction parameters. We have used here the same parameters as in the work by Ravikovitch *et al.*[47] who, in Fig. 5 of their paper, show experimental, GCMC and nonlocal DFT (NLDFT)[15] adsorption isotherm results. As seen in Fig. 10, it is remarkable that the behavior predicted by our calculations quantitatively agrees with the experimental and simulation results shown in this reference. However, the adsorption isotherm predicted by NLDFT shows steps indicating a layering pattern not present in the experimental data. Our FMT calculations are in good agreement with their GCMC results at low pressures and show a less pronounced layering than that of Ravikovitch *et al.*[47]

IV. CONCLUSIONS

In this work we have analyzed the ability of the FMT due to Kierlik and Rosinberg in predicting adsorption isotherms as well as density profiles in cylindrical pores, by comparison with data obtained from GCMC using the same molecular model. This work is of relevance in the context of the use of DFT calculations for the determination of pore-size distributions from experimentally obtained adsorption isotherms.

A comparison of FMT for cylindrical pores with GCMC simulations has shown a very good agreement for the range of pore sizes studied, confirming the ability of the theory in the description of nearly one-dimensional confined systems. The exact limit of its validity for very narrow pores lies beyond the scope of this work.

Our results indicate that a layering behavior takes place in the smallest cylindrical pore considered, $H=3.2\,\sigma$, while the adsorption in a planar pore of the same size needs a much higher chemical potential to achieve a significant adsorption. As the pore size increases, the influence of the geometry becomes less important, although a certain shift in the capillary condensation transition can still be observed. Additionally, for wider pores, such as $H=8.8\,\sigma$ and $17.8\,\sigma$, we obtain multilayer adsorption with capillary condensation at high chemical potentials, with the same qualitative behavior observed for both geometries. When the diameter size reaches the limit where the curvature effects are not of further relevance, the cylindrical pores reduce to the same quantitative behavior as the slitlike pores.

The formation of a thin adsorbed layer at intermediate and large pore sizes seems to correspond to a thermodynamic second order phase transition, for the range of parameters used and the thermodynamic conditions studied. However, the results found seem to indicate some relationship between this behavior and the prewetting transition observed in semi-infinite geometries, especially in the neighborhood of the critical end point of the prewetting line. The effect of the confinement is very important in this crossover behavior. In fact, the local curvature of the solid wall is the only responsible for the shift observed in cylindrical geometries in our study, although a deeper analysis is required to shed some light on this particular point.

From the comparison of FMT calculations versus NLDFT results, we conclude that the FMT is an excellent tool for the study of the behavior of fluids in confined cylindrical geometries. However, a systematic comparison between results obtained by two DFT versions in cylindrical pores would be necessary, and constitutes an interesting subject for future work.

ACKNOWLEDGMENTS

The authors thank Lev D. Gelb and Keith E. Gubbins for useful discussions. Alexander V. Neimark, Peter I. Ravikovitch, and Aleksey Vishnyakov are gratefully acknowledged for providing data for Fig. 10. This work was supported by the Spanish Government Ministerio de Ciencia y Tecnología (Grant Nos. PPQ2000-2888-E, PPQ2001-0671) and by URV (Project No. 2000PIR-21). S.F-G. thanks URV (Spain) and CONACyT (México) for financial support. F.J.B. thanks the Universidad de Huelva and the Junta de Andalucía for financial support.

APPENDIX: GEOMETRICAL DETAILS

The inversion of Eq. (5) in cylindrical pores requires the calculation of a series of convolutions, generically expressed as

$$\int d\mathbf{r}\,\psi(|\mathbf{r}-\mathbf{r}''|)f(\mathbf{r}), \tag{A1}$$

where $\psi(|\mathbf{r}|)$ is an arbitrary isotropic kernel, and $f(\mathbf{r})$ a given function of the position which, for symmetry requirements, depends only on the distance to the axis of the cylin-

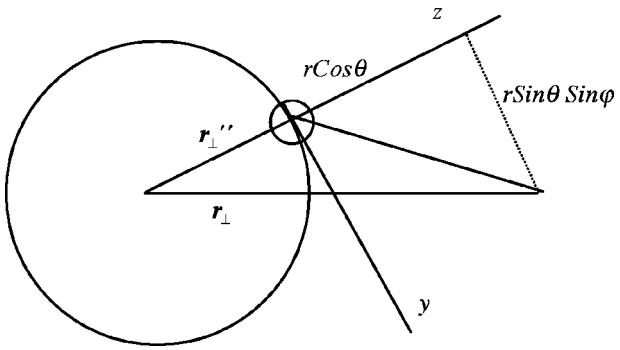

FIG. 11. Projection of the cylindrical pore on a plane orthogonal to cylinder axis following Eq. (A2).

der $\mathbf{r}_\perp$. Identically and also due to symmetry requirements, the result of each of these convolutions is a function of the distance to the axis of the cylinder, $\mathbf{r}''_\perp$.

To take advantage of the isotropy of the kernel, we have introduced a local coordinate system around the space point $\mathbf{r}''$. The *z* axis is perpendicular to the cylinder's axis pointing outward in the radial direction, the *y* axis is parallel to the cylinder's axis, and the *x* axis is correspondingly oriented (see Fig. 11). Adopting spherical coordinates with respect to this local reference system, the distance $\mathbf{r}_\perp$ of a given space point can be obtained according to the transformation

$$r_\perp(r,\ \theta,\ \varphi;\ r''_\perp)=\sqrt{(r''_\perp+r\cos\theta)^2+r^2\sin^2\theta\sin^2\varphi}, \tag{A2}$$

which permits the evaluation of the function $f(\mathbf{r}_\perp)$. The convolutions are then calculated by repeated one-dimensional integration, taking advantage of Gaussian quadratures to increase the velocity of the numerical evaluation. We have not introduced here a reduction of the multidimensional integration by an appropriate (although cumbersome for nonplanar geometries) coordinate change, as it is the case in the adsorption on a flat wall.[23] However, there is not a significant increase in the computational time, since the problem is still onedimensional, due to the fact that the density profile is a function which depends only on the distance to the axis of the cylinder, $\mathbf{r}_\perp$. As a result, the comparison between the density profiles in slitlike and cylindrical pores shows significant differences near the axial region due, precisely, to these curvature effects.

[1] L. D. Gelb, K. E. Gubbins, R. Radhakrishnan, and M. Sliwinska-Bartkowiak, Rep. Prog. Phys. **62**, 1573 (1999).
[2] R. Evans, in *Fundamentals of Inhomogeneous Fluids*, edited by D. Henderson (Dekker, New York, 1992), Chap. 3, p. 85.
[3] D. E. Sullivan and M. M. Telo da Gama, in *Fluid Interfacial Phenomena*, edited by C. A. Croxton (Wiley, New York, 1986), Chap. 2, p. 45.
[4] S. Dietrich, in *Phase Transitions and Critical Phenomena*, edited by C. Domb and J. L. Lebowitz (Academic, New York, 1988), Vol. 12, Chap. 1, p. 1.
[5] R. Evans, J. Phys.: Condens. Matter **2**, 8989 (1990).
[6] P. Tarazona and R. Evans, Mol. Phys. **48**, 799 (1983).
[7] P. Tarazona, M. M. Telo da Gama, and R. Evans, Mol. Phys. **49**, 283 (1983).
[8] P. Tarazona and R. Evans, Mol. Phys. **47**, 1033 (1982).
[9] R. Evans and A. O. Parry, J. Phys.: Condens. Matter **1**, 7207 (1989).
[10] S. Nordholm, M. Johnson, and B. C. Freasier, Aust. J. Chem. **33**, 2139 (1980).
[11] M. Johnson and S. Nordholm, J. Chem. Phys. **75**, 1953 (1981).
[12] B. C. Freasier and S. Nordholm, J. Chem. Phys. **79**, 4431 (1983).
[13] B. C. Freasier and S. Nordholm, Mol. Phys. **54**, 33 (1986).
[14] P. Tarazona, Mol. Phys. **52**, 81 (1984).
[15] P. Tarazona, Phys. Rev. A **31**, 2672 (1985); **32**, 3148(E) (1985).
[16] W. A. Curtin and N. W. Ashcroft, Phys. Rev. A **32**, 2909 (1985).
[17] T. F. Meister and D. M. Kroll, Phys. Rev. A **31**, 4055 (1985).
[18] J. K. Percus, J. Stat. Phys. **28**, 67 (1982).
[19] J. K. Percus, J. Chem. Phys. **75**, 1316 (1981).
[20] J. K. Percus, J. Stat. Phys. **52**, 1157 (1988).
[21] A. Robledo and C. Varea, J. Stat. Phys. **26**, 513 (1981).
[22] Y. Rosenfeld, Phys. Rev. Lett. **63**, 980 (1989).
[23] E. Kierlik and M. L. Rosinberg, Phys. Rev. A **42**, 3382 (1990).
[24] S. Phan, E. Kierlik, M. L. Rosinberg, B. Bildstein, and G. Kahl, Phys. Rev. E **48**, 618 (1993).
[25] R. Evans and P. Tarazona, Phys. Rev. Lett. **52**, 557 (1984).
[26] R. Evans and U. Marini Bettolo Marconi, Chem. Phys. Lett. **114**, 415 (1985).
[27] R. Evans and U. Marini Bettolo Marconi, Phys. Rev. A **32**, 3817 (1985).
[28] B. K. Peterson, J. P. R. B. Walton, and K. E. Gubbins, Int. J. Thermophys. **6**, 585 (1985).
[29] R. Evans, U. Marini Bettolo Marconi, and P. Tarazona, J. Chem. Phys. **84**, 2376 (1986).
[30] R. Evans, U. Marini Bettolo Marconi, and P. Tarazona, J. Chem. Soc., Faraday Trans. 2 **82**, 1763 (1986).
[31] B. K. Peterson, J. P. R. B. Walton, and K. E. Gubbins, J. Chem. Soc., Faraday Trans. 2 **82**, 1789 (1986).
[32] P. Tarazona, U. Marini Bettolo Marconi, and R. Evans, Mol. Phys. **60**, 573 (1987).
[33] R. Evans and U. Marini Bettolo Marconi, J. Chem. Phys. **86**, 7138 (1987).
[34] B. K. Peterson, K. E. Gubbins, G. S. Heffelfinger, U. Marini Bettolo Marconi, and F. van Swol, J. Chem. Phys. **88**, 6487 (1988).
[35] B. K. Peterson, G. S. Heffelfinger, K. E. Gubbins, and F. van Swol, J. Chem. Phys. **93**, 679 (1990).
[36] P. B. Balbuena and K. E. Gubbins, Langmuir **9**, 1801 (1993).
[37] C. Lastoskie, K. E. Gubbins, and N. Quirke, Langmuir **9**, 2693 (1993).
[38] E. Kierlik and M. L. Rosinberg, Phys. Rev. A **44**, 5025 (1991).
[39] E. Kierlik, M. L. Rosinberg, J. E. Finn, and P. A. Monson, Mol. Phys. **75**, 1435 (1992).
[40] E. Kierlik, M. L. Rosinberg, Y. Fan, and P. A. Monson, J. Chem. Phys. **101**, 10947 (1994).
[41] S. Jiang, K. E. Gubbins, and P. B. Balbuena, J. Phys. Chem. **98**, 2404 (1994).
[42] S. Phan, E. Kierlik, M. L. Rosinberg, A. Yethiraj, and R. Dickman, J. Chem. Phys. **102**, 2141 (1995).
[43] E. Kierlik, Y. Fan, P. A. Monson, and M. L. Rosinberg, J. Chem. Phys. **102**, 3712 (1995).
[44] S. L. Sowers and K. E. Gubbins, Langmuir **11**, 4758 (1995).
[45] M. Sliwinska-Bartkowiak, S. L. Sowers, and K. E. Gubbins, Langmuir **13**, 1182 (1997).
[46] P. Bryk, W. Cyrankiewicz, M. Borowko, and S. Sokołowski, Mol. Phys. **93**, 111 (1998).
[47] P. I. Ravikovitch, A. Vishnyakov, and A. V. Neimark, Phys. Rev. E **64**, 011602 (2001).
[48] A. González, J. A. White, F. L. Román, and R. Evans, J. Chem. Phys. **109**, 3637 (1998).
[49] Y. Rosenfeld, M. Schmidt, H. Löwen, and P. Tarazona, Phys. Rev. E **55**, 4245 (1997).
[50] P. Tarazona, Phys. Rev. Lett. **84**, 694 (2000).
[51] S. J. Gregg and K. S. W. Sing, Adsorption, Surface Area and Porosity, 2nd ed. (Academic, London, 1982), Chap. 3, p. 132.
[52] H. Reiss, H. L. Frisch, and J. L. Lebowitz, J. Chem. Phys. **31**, 369 (1959).
[53] E. Helfand, H. L. Frisch, and J. L. Lebowitz, J. Chem. Phys. **34**, 1037 (1961).
[54] R. Evans, Adv. Phys. **28**, 143 (1979).
[55] L. D. Gelb and K. E. Gubbins, Langmuir **14**, 2097 (1998).
[56] L. D. Gelb and K. E. Gubbins, Langmuir **15**, 305 (1999).
[57] M. W. Maddox, J. P. Olivier, and K. E. Gubbins, Langmuir **13**, 1737 (1997).
[58] J. D. Weeks, D. Chandler, and H. C. Andersen, J. Chem. Phys. **54**, 5237 (1971).
[59] L. Verlet and J. J. Weis, Phys. Rev. A **5**, 939 (1972).
[60] B. Q. Lu, R. Evans, and M. M. Telo da Gama, Mol. Phys. **55**, 1319 (1985).
[61] M. S. Wertheim, Phys. Rev. Lett. **10**, 321 (1963).

[62] E. Thiele, J. Chem. Phys. **39**, 474 (1963).
[63] J. L. Lebowitz, Phys. Rev. **133**, A895 (1964).
[64] A. Brodka and T. W. Zerda, J. Chem. Phys. **95**, 3710 (1991).
[65] J. M. D. MacElroy, Langmuir **9**, 2682 (1993).
[66] P. I. Ravikovitch, A. Vishnyakov, R. Russo, and A. V. Neimark, Langmuir **16**, 2311 (2000).
[67] M. P. Allen and D. J. Tildesley, *Computer Simulation of Liquids* (Clarendon, Oxford, 1987), Chap. 4, p. 110.
[68] D. Frenkel and B. Smit, *Understanding Molecular Simulation: from Algorithms to Applications* (Academic, San Diego, 1996), Chap. 3, p. 19.
[69] P. C. Ball and R. Evans, J. Chem. Phys. **89**, 4412 (1988).
[70] C. Lastoskie, K. E. Gubbins, and N. Quirke, J. Phys. Chem. **97**, 4786 (1993).
[71] J. S. Rowlinson and B. Widom, *Molecular Theory of Capillarity* (Clarendon, Oxford, 1984).
[72] G. J. Tjatjopoulos, D. L. Feke, and J. A. Mann, Jr., J. Phys. Chem. **92**, 4006 (1988).
[73] W. H. Press, S. A. Teukolsky, W. T. Vetterling, and B. P. Flannery, *Numerical Recipes in Fortran*, 2nd ed. (Cambridge University Press, Cambridge, 1992), Chap. 6, p. 263.
[74] J. H. Deboer, B. G. Linsen, and T. J. Osinga, J. Catal. **4**, 643 (1965).